JACS
JOURNAL OF THE AMERICAN CHEMICAL SOCIETY

Article

pubs.acs.org/JACS

The Electronic Influence of Abasic Sites in DNA

Marc A. McWilliams, Rita Bhui, David W. Taylor, and Jason D. Slinker*

Department of Physics, The University of Texas at Dallas, 800 W. Campbell Rd., PHY 36, Richardson, Texas 75080, United States

Supporting Information

ABSTRACT: Abasic sites in DNA are prevalent as both naturally forming defects and as synthetic inclusions for biosensing applications. The electronic impact of these defects in DNA sensor and device configurations has yet to be clarified. Here we report the effect of an abasic site on the rate and yield of charge transport through temperature-controlled analysis of DNA duplex monolayers on multiplexed devices. Transport yield through the abasic site monolayer strongly increases with temperature, but the yield relative to an undamaged monolayer decreases with temperature. This is opposite to the increasing relative yield with temperature from a mismatched base pair, and these effects are accounted for by the unique structural impact of each defect. Notably, the effect of the abasic site is nearly doubled when heated from room temperature to 37 °C. The rate of transport is largely unaffected by the abasic site, showing Arrhenius-type behavior with an activation energy of ∼300 meV. Detailed abasic site investigation elucidates the electrical impact of these biologically spontaneous defects and aids development of biological sensors.

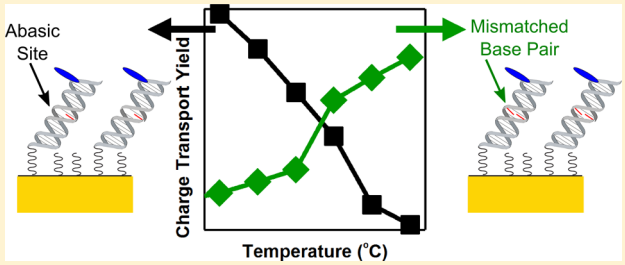

INTRODUCTION

Apurinic/apyrimidic or abasic sites are formed hundreds to thousands of times per day in a given cell, both spontaneously and as a result of DNA damage repair processes.[1] Following the formation of abasic sites is thus fundamental to the understanding of cellular activity. In addition, synthetic incorporation of abasic sites is also of interest in the development of biosensors.[2,3] Multiple works now show the utility of abasic sites within surface-bound DNA constructs for storage of displaceable fluorescent or electrochemical probes for selective detection of analytes.[4−11] For other sensors, the presence of an abasic site or the creation of one by DNA repair processes triggers an optical or electrical transduction event.[12−18] Thus, the utilization and formation of abasic sites within DNA have great significance in natural and synthetic biology.

Abasic sites have also been shown to dramatically influence charge-transport (CT) processes through DNA itself. In most cases, abasic sites produced a lowering of the yield of CT.[7,19−23] Practically, electrical and electrochemical sensors utilizing DNA CT are sensitive to abasic sites, enabling the precise study of DNA base-excision and damage repair at the level of DNA.[13,14,22,24] Fundamentally, since DNA CT is understood to proceed through the π-stacked orbitals of the bases,[23] the presumed CT implication of the removal of a base is the breaking of the continuity of the base pair π-stacking. However, study of the effects of abasic sites on CT kinetics has not been reported. Detailed investigation of an abasic site elucidates the electrical impact of these naturally occurring defects and aids the continued development of electrical and electrochemical biological sensors for DNA damage and DNA damage repair.

Here we report the effect of abasic site incorporation on the rate and yield of CT relative to undamaged and mismatch-containing duplexes through surface-bound DNA electrochemistry on multiplexed chips. This approach enables direct temperature-controlled comparison under biologically relevant conditions with redundancy and ensures identical assembly and testing conditions for each sequence. The implications for biosensing and understanding of fundamental DNA CT are discussed.

EXPERIMENTAL SECTION

Synthesis of Oligonucleotides. Thiolated sequences were obtained from Integrated DNA Technologies (IDT) or synthesized on an Applied Biosystems (ABI) 394 DNA Synthesizer. The abasic sites and thiol linkers were incorporated with the Glen Research dSpacer and thiol-modifier C6 S-S phosphoramidites, respectively. The DNA containing the Nile blue precursor base, a 5-[3-acrylate NHS ester] deoxyuridine phosphoramidite from Glen Research, was purchased from Trilink BioTechnologies, and the dye covalently coupled under ultramild conditions according to established procedures.[25]

Purification and Characterization of Oligonucleotides. All oligonucleotides were purified via two rounds of high-performance liquid chromatography on a Shimadzu LC-20AD instrument outfitted with an SIL-20A autosampler and an SPD-M20A diode array detector. In the first purification round, DNA oligonucleotides with the 4,4′-dimethoxytrityl group on were eluted on a gradient that was evolved from 5% acetonitrile and 95% 50 mM ammonium acetate, pH = 8 buffer to 75% acetonitrile and 25% 50 mM ammonium acetate, pH = 8 buffer over 30 min. In the second purification round, DNA oligonucleotides with the 4,4′-dimethoxytrityl group off (removed according to Glen Research procedures for each strand) were eluted on a gradient that was evolved from 5% acetonitrile and 95% 50 mM

Received: June 25, 2015
Published: August 17, 2015

DOI: 10.1021/jacs.5b06604
J. Am. Chem. Soc. 2015, 137, 11150−11155

ammonium acetate, pH = 8 buffer to 15% acetonitrile and 85% 50 mM ammonium acetate, pH = 8 buffer over the first 35 min; from 15% acetonitrile and 85% 50 mM ammonium acetate, pH = 8 buffer to 50% acetonitrile and 50% 50 mM ammonium acetate, pH = 8 buffer over the next 5 min; and finally, held constant at 50% acetonitrile for another 5 min. The identity of the desired products was confirmed by matrix-assisted laser desorption ionization time-of-flight mass spectrometry on a Shimadzu Axima Confidence mass spectrometer.

Preparation of Duplex DNA. The oligonucleotides were quantified via UV−vis spectroscopy on a Beckman DU-800 UV−visible spectrophotometer. Duplex DNA was prepared by mixing equimolar amounts of complementary strands and annealing the solution to 95 °C, followed by slow cooling to room temperature over a period of 90 min. The formation of duplex DNA was verified by temperature-dependent absorbance measurements and melting temperature analysis (see Supporting Information Figure 2).

Fabrication of Multiplexed Gold Electrodes. The chips/substrates featuring multiplexed gold electrodes for DNA self-assembly and electrochemical experiments were prepared as previously described.[14] In brief, 1 mm thick Si wafers featuring a 10 000 Å thick oxide layer (Silicon Quest, Inc.) were patterned via a two-layer process. For the first layer, the gold electrodes were deposited by a lift-off technique. Initially, the wafers were cleaned thoroughly in 1165 Remover (Microchem, Inc.) to remove organic impurities. SPR 220 3.0 photoresist (Microchem, Inc.) was then spin-cast at 2000 rpm onto the wafers and baked. The photoresist was in turn patterned with a Karl Suss MA6 contact aligner and a chrome photomask. Following post-exposure baking, the wafers were developed in AZ 300 MIF developer for 1 min and rinsed thoroughly with deionized water. A 100 Å Ti adhesion layer and a 1000 Å Au layer were deposited onto the wafers via electron beam physical vapor deposition. The wafers were then immersed in Remover PG (Microchem, Inc.) overnight and sonicated to complete metal lift-off. Subsequently, the wafers were baked again and cleaned by UV ozone treatment. For the second layer, SU-8 2002 photoresist was spin-cast onto the wafers at 3000 rpm, baked, and photopatterned as an insulator, thereby isolating the exposed gold working electrode areas from the contact pads. The wafers were then developed in SU-8 Developer (Microchem, Inc.) for 1 min and baked to permanently set the photoresist. Finally, the completed wafers were diced into 1 × 1 in. chips by hand with a diamond scribe and stored under vacuum. The resulting multiplexed electrodes allowed for the self-assembly of four distinct DNA monolayers, each with 4-fold redundancy, on a single chip/substrate, facilitating direct, unambiguous comparisons between different DNA monolayers.

Self-Assembly of DNA Monolayers. The DNA monolayers were self-assembled onto gold electrode pads from a 5 mM phosphate, 50 mM sodium chloride, pH = 7 buffer solution supplemented with 50 mM Mg^{2+} over a period of 12−18 h. The substrates were backfilled with mercaptohexanol for 1 h to remove nonspecifically bound DNA and then thoroughly rinsed with buffer to remove residual mercaptohexanol.

Electrochemistry of DNA Monolayers. The multiplexed substrates were placed in the custom mount shown in Supporting Information Figure 1, which was connected to electrochemical testing hardware (a CH Instruments CHI750D Electrochemical Analyzer and a CHI 684 Multiplexer). The electrochemical measurements were performed in 5 mM phosphate, 50 mM sodium chloride, pH = 7 buffer with 4 mM spermidine. For experiments requiring temperature variation, the entire mount was placed in a previously reported custom copper enclosure, which was in turn submerged in a recirculating water bath, as shown in Supporting Information Figure 1.

RESULTS AND DISCUSSION

To follow the effect of an abasic site, we designed, synthesized, and purified the DNA duplexes illustrated in Figure 1. The DNA duplexes consisted of two complementary 17-mer oligonucleotides: one functionalized with a single Nile blue-modified thymidine at the 5′ terminus, and the other with an

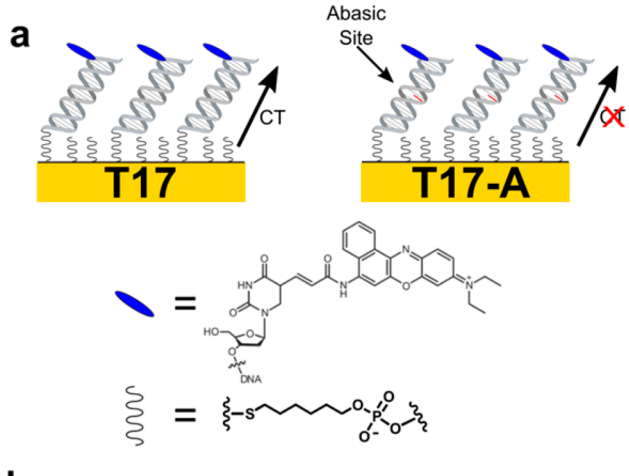

Name	Strand	Sequence
T17	Probe	3′-CTCTATATTTCGTGCGT$_{NB}$-5′
	Thiol	5′-GAGATATAAAGCACGCA-3′
T17-A	Probe	3′-CTCTATATTTCGTGCGT$_{NB}$-5′
	Thiol	5′-GAGATA_AAAGCACGCA-3′

Figure 1. Illustration and sequence descriptions of the well-matched and abasic site monolayers used in this study. (a) An illustration of the well-matched and abasic DNA monolayers used in this study. The **T17** monolayer is a well-matched, defect-free 17mer duplex, and **T17-A** is a 17mer duplex with a single abasic site. The Nile blue and thiol modifiers are also shown. (b) The sequences for the **T17** and **T17-A** monolayers.

alkanethiol linker at its 5′ terminus (Figure 1). One of the thiol-modified nucleotides was prepared fully complementary to the Nile blue-modified strand, labeled **T17** due to the distal position of the probe relative to the electrode. The other thiolated strand was prepared with a single abasic site near the middle of the duplex, labeled **T17-A**. These hybridized duplexes were self-assembled into DNA monolayers on multiplexed gold electrodes in the presence of excess Mg^{2+}. Such DNA monolayers are known to be densely packed, with the DNA adopting an upright orientation relative to the electrode surface. The surface concentration of these duplexes under these conditions is estimated to be approximately 20 pmol/cm^2, correlating with an approximate nearest-neighbor distance of 3 nm.[26] This dense packing of the DNA monolayers ensures that the electrochemical properties primarily reflect charge-transfer mediated by the DNA base pair stack, rather than mechanical motion of the DNA.[27,28]

We first investigated the room temperature cyclic voltammetry (CV) of DNA monolayers from the **T17** and **T17-A** DNA duplexes illustrated in Figure 1, that is, fully well-matched duplexes and duplexes containing a single abasic site. Figure 2 shows typical cyclic voltammograms obtained from each of these sequences at a scan rate of 100 mV/s. These two monolayers displayed a redox couple with a cathodic peak near −0.250 V vs Ag/AgCl that could be assigned to quasi-reversible reduction of the Nile blue redox probe.[25,26,28−32] The fully well-matched **T17** monolayer exhibited cathodic CV peak heights and areas of 10.3 nA and 8.4 nC, respectively, while the abasic containing **T17-A** monolayer yielded a peak height of 3.7 nA and an area of 2.6 nC. These peak heights and areas are proportional to the yield of the CT process to the DNA probe through the DNA monolayer. These metrics of CT yield show

DOI: 10.1021/jacs.5b06604
J. Am. Chem. Soc. 2015, 137, 11150−11155

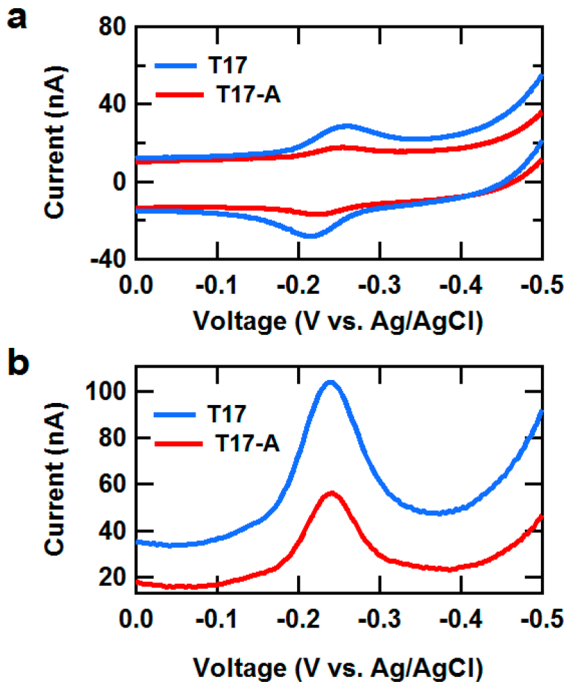

Figure 2. Representative cyclic and square wave voltammograms for well-matched and abasic site DNA monolayers. (a) CV (100 mV/s) and (**b**) SWV (40 Hz) curves for **T17** and **T17-A** DNA duplexes at room temperature.

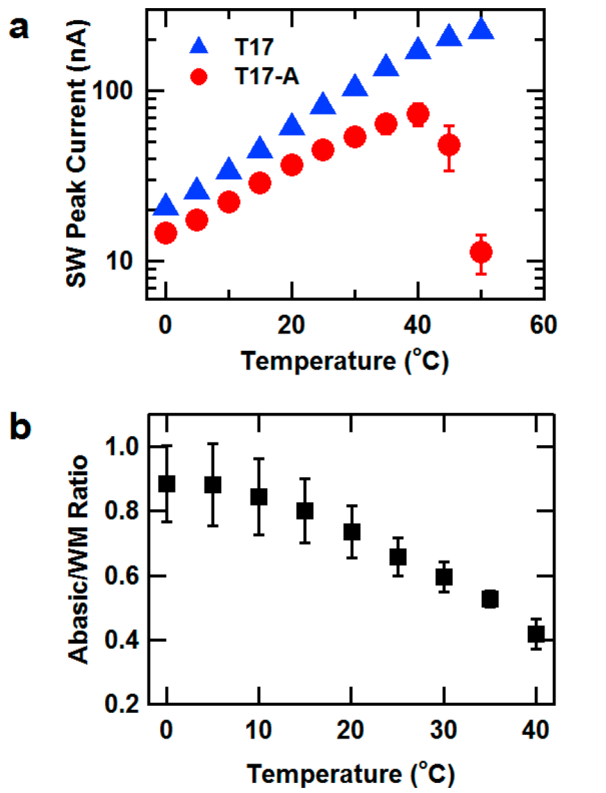

Figure 3. Charge-transfer yields versus temperature for well-matched and abasic site DNA monolayers. (a) Logarithmic plot of SWV peak current versus temperature for well-matched (T17) and single abasic site (T17-A) DNA monolayers from a single chip. Error bars represent the standard deviation across four electrodes. (b) The ratio of well-matched to abasic SWV peak current with temperature, averaged across three experimental comparisons of each monolayer on the same chip. Error bars represent the standard error across the three trials.

that the presence of the abasic site attenuates this yield by approximately a factor of 3, consistent with prior reports of electrochemical measurements of abasic sites.[19,24]

Similarly, we investigated the room-temperature square wave voltammetry (SWV) from **T17** and **T17-A** monolayers, as SWV minimizes background capacitive contributions to the current and provides more sensitivity to the surface-bound peak.[33] SWV peak heights (taken at 25 mV amplitude and 15 Hz), another estimation of CT yield, for **T17** and **T17-A** monolayers at room temperature were 62 and 36 nA, respectively, again showing consistency with the Nile blue probe as well as significant attenuation due to the abasic site. The inclusion of the abasic site dramatically lowers the UV–vis melting temperature (from 64 to 52 °C, see Supporting Information Figure 2), a metric of the DNA duplex stability. Thus, the lower values of CT yield through abasic site monolayers as estimated by CV and SWV follow the observed trend that yield is proportional to the stability of the duplex.[28,34]

To further explore the nature of the attenuation of CT yield by an abasic site, we followed the temperature dependence of the square wave peak height from 0 °C (near the freezing point of the buffer) up through 55 °C, which is beyond the melting transition of the **T17-A** duplex where the probe strand will no longer be bound to the duplex (Figure 3A). This figure represents peak heights averaged across the **T17** and **T17-A** monolayers of a single chip and hence compares the monolayers under the same assembly and environmental conditions. For the fully well-matched **T17** duplex, the yield increases dramatically, over an order of magnitude, consistent with our prior measurement.[26] This supports the understanding that only a fraction of the duplexes of the monolayer are redox active (the total surface coverage has been estimated to be ~20 pmol/cm^2) and that this fraction increases significantly with temperature.[26] Similarly, the **T17-A** monolayer also increases with temperature, up to about 40 °C, where the peak height begins to drop. This sharp drop correlates with the onset of the melting transition of this monolayer, consistent with prior reports (see Supporting Information Figure 2).[26,28] Detailed comparison of the **T17** and **T17-A** monolayers reveals that the **T17-A** sequence SWV peak height grows at a slower rate. To ensure the consistency of this trend of CT yield with temperature, we measured the SWV peak heights with temperature from additional **T17** and **T17-A** monolayers prepared on the same chips (three trials). In Figure 3B, the ratio of SWV peak heights for **T17-A** to **T17** monolayers (Abasic/WM ratio) versus temperature is shown, clearly revealing a decreasing trend. This trend was also observed to hold in CV peak heights, an additional measure of CT yield (see Supporting Information Figure 3). Thus, the yield of transport through an abasic site appears to decrease with temperature relative to a fully well-matched monolayer.

This trend of CT yield ratio with temperature has important implications when compared to other naturally occurring defects, such as mismatched base pairs. The decreasing abasic to well-matched CT yield ratio is in stark contrast to that observed with mismatch containing DNA, where the mismatch to well-matched CT yield ratio increases with increasing temperature, as seen in both in electrochemical and photoluminescence studies.[26,35] To verify the different impacts of these defects, we prepared a duplex containing a single base pair

DOI: 10.1021/jacs.5b06604
J. Am. Chem. Soc. 2015, 137, 11150–11155

mismatch, **T17-MM**, which used the same probe strand as in Figure 1 and a thiol strand of 5′-GAG ATA CAA AGC ACG CA-3′, where C is the location of a CA mismatch. Similar to the abasic site, the mismatch also significantly decreases the melting temperature of the duplex (from 64 to 56 °C). We subsequently tested well-matched (**T17**), single base pair mismatch (**T17-MM**) and abasic site (**T17-A**) monolayers on the same chip and measured SWV peak height of each defect containing monolayer against that of the well-matched monolayer (Defect/WM ratio, Figure 4). The trend of

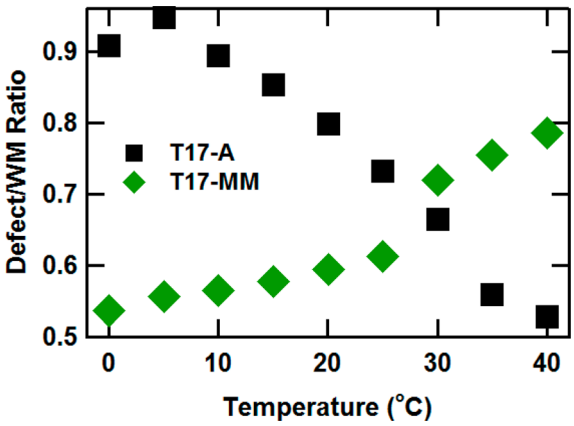

Figure 4. Relative charge-transfer yields versus temperature for DNA monolayers containing abasic or mismatch sites. The ratio of SWV peak current with temperature comparing monolayers containing either a single base pair mismatch (T17-MM) or a single abasic site (T17-A) against fully well-matched DNA monolayers (T17), averaged across a single chip (four electrodes each).

increasing ratio held for the abasic defect, and a trend of decreasing ratio emerged for the mismatch, consistent with the prior report.[26] Notably, though both defects produce significant attenuation in the stability of the duplex, the electronic impact of each is expressed very differently with temperature.

Detailed analysis of the structures of abasic and CA mismatch duplexes can account for the distinct temperature dependence of the CT yield ratios for the **T17-A** and **T17-MM** monolayers. Studies of the equilibrium conformation of abasic-containing DNA in various sequence contexts reveal that, for an abasic site opposite an adenine, the adenine remains well-stacked in virtually the same position as it would across from a thymine, with very little distortion of the surrounding duplex.[36−40] Temperature likely then disrupts this delicate balance as thermal motion may cause the unpaired adenine to swing out of the double helix, bringing about losses in the π-stacking, with no restoring force from base-pairing. Similarly, CA mismatches do not typically affect the global structure of the double helix, and crystal structures show the base pair to fall within the π-stack.[41] However, for pH 7 and above, the N_1 atom of the adenine in the mismatch is not likely to be protonated, compromising the hydrogen bonding between the atoms.[42,43] This allows for "propeller twisting" of the bases relative to one another,[44] as evidenced in the crystal structure[41] decreasing the overlap with the π-stack of the overall double helix. This effect would compromise CT at low temperatures. Unlike the abasic site, however, the remaining hydrogen bond between the bases will tend to maintain the CA mismatch within the π-stack with thermal fluctuations, allowing for improved CT with temperature before the melting transition.

We subsequently analyzed the SWV curves of the **T17-A** against **T17** monolayers to extract the rate of electron transfer k according to a method similar to that first described by O'Dea and Osteryoung[45] using a modified Nelder−Mead simplex algorithm from our laboratory. The extracted transfer rates versus temperature are plotted in Figure 5. Very little difference

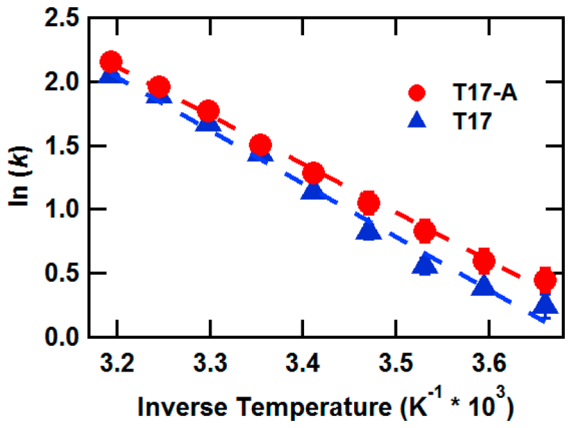

Figure 5. Charge-transfer rates for abasic and well-matched monolayers. An Arrhenius-type plot of the natural logarithm of the electron-transfer rate k as a function of the inverse temperature for **T17-A** (24 electrodes over 3 chips) against a co-tested **T17** control. The dashed line represents a least-squares fit of the data.

is seen between the **T17** and **T17-A** rates, which vary between 1 and 10 s^{-1} from 0 to 40 °C. These rates are consistent with those reported for Nile blue-modified monolayers[26,28,29] and a rate-limiting linker.[46] Previously, we demonstrated that the rate of CT (k) of the **T17** monolayer, as well as others tested to date, follows Arrhenius-like behavior over a 0−35 °C temperature range:

$$k(T) \propto \exp(-E_A/k_B T)$$

where E_A is the activation energy, k_B is the Boltzmann constant, and T is temperature.[26,28,34] As seen in prior works, Arrhenius behavior is again observed for the **T17** monolayer, and now demonstrated here for the **T17-A** monolayer. Very little difference is seen, indicating that the states primarily responsible for efficient CT are similar in each monolayer. As the CT yield results were rationalized in view of the structure of the π-stacked bases, it follows that the necessary conformations for appreciable conductivity are similar for each and could give rise to this equivalency. An average activation energy of 326 ± 6 meV was observed for **T17-A** monolayers. A similar value for E_A was also found for **T17**, which is higher than previously reported for Nile blue monolayers[26,28] and similar constructs,[34,47,48] but closer to theoretically anticipated values for CT through DNA.[49,50] Laviron analysis of the **T17-A** monolayer was also performed and found to give similar rate results (see Supporting Information Figure 4).

It should be noted that we have previously shown the transfer rates of **T17** and **T17-MM** monolayers to be comparable.[26] To verify similar kinetic behavior, we also measured the transfer rates of **T17-A** against **17-MM** with temperature and observed similar rates (see Supporting Information Figure 5). Overall, these observations are consistent with prior reports of temperature-activated CT through DNA.[26,28]

DOI: 10.1021/jacs.5b06604
J. Am. Chem. Soc. 2015, 137, 11150−11155

CONCLUSIONS

Our results inform the design of sensors that rely on generation of an abasic site for signal transduction. Greater discrimination of an abasic site versus a well-matched monolayer will occur with higher temperatures. For example, interpolating our data from Figure 3b, when temperature is increased from room temperature to 37 °C (physiological temperature) the Abasic/WM ratio decreases from 0.71 to 0.48, improving discrimination by 83%. Thus, a relatively small temperature change nearly doubles the impact of the abasic site. This is fortuitous for studies involving the creation of an abasic site by proteins and enzymes, whose activity is often optimized at 37 °C. Longer lengths of DNA or increased GC content for each duplex would raise the melting temperature and perhaps enable even greater discrimination.

In conclusion, relative to a fully well-matched duplex, the abasic site lowers the yield of CT, and the WM/Abasic ratio is increased with temperature. It follows that DNA biosensing events depending on the formation of an abasic site for signal transduction will give the greatest relative changes at higher temperatures. Furthermore, the trend of increasing relative attenuation of CT with temperature and its stark contrast with a mismatch inclusion speaks for its intricate connection to the structure of the DNA duplex and particularly its dependence on the structure of the DNA base pair π-stack. The virtual lack of impact of the abasic site on the rate of CT indicates similarity in transport active states in these constructs with undamaged monolayers. This detailed investigation of an abasic site elucidates the electrical impact of these biologically spontaneous defects and aids the continued development of electrical and electrochemical biological sensors for DNA damage and DNA damage repair.

ASSOCIATED CONTENT

Supporting Information

The Supporting Information is available free of charge on the ACS Publications website at DOI: 10.1021/jacs.5b06604.

Images of custom temperature controlled electrochemical setup, melting curves of DNA monolayers, CV analysis of yield ratios, Laviron analysis of transfer rates, and temperature-dependent rate comparisons of defect monolayers (PDF)

AUTHOR INFORMATION

Corresponding Author

*slinker@utdallas.edu

Notes

The authors declare no competing financial interest.

ACKNOWLEDGMENTS

This work was supported by the National Science Foundation (CMMI-1246762) and funds from both startup support from UT Dallas and a gift from Plexon, Inc. The authors would like to thank the group of A. Gorodetsky for synthesis of some of the DNA used in this study, X. Liu for his role in fabrication of the chips, and D. Kahanda and Y. Zhu for assistance with experiments.

REFERENCES

(1) Wilson, D. M.; Barsky, D. *Mutat. Res., DNA Repair* **2001**, *485*, 283.
(2) Palecek, E.; Bartosik, M. *Chem. Rev.* **2012**, *112*, 3427.
(3) Sontz, P. A.; Muren, N. B.; Barton, J. K. *Acc. Chem. Res.* **2012**, *45*, 1792.
(4) Roy, J.; Chirania, P.; Ganguly, S.; Huang, H. *Bioorg. Med. Chem. Lett.* **2012**, *22*, 863.
(5) Shao, Y.; Morita, K.; Dai, Q.; Nishizawa, S.; Teramae, N. *Electrochem. Commun.* **2008**, *10*, 438.
(6) Shao, Y.; Niu, Z.; Zou, S. *Electrochem. Commun.* **2009**, *11*, 417.
(7) Buzzeo, M. C.; Barton, J. K. *Bioconjugate Chem.* **2008**, *19*, 2110.
(8) Ahn, J. K.; Park, K. S.; Won, B. Y.; Park, H. G. *Biosens. Bioelectron.* **2015**, *67*, 590.
(9) Huang, W.; Morita, K.; Sankaran, N. B.; Nishizawa, S.; Teramae, N. *Electrochem. Commun.* **2006**, *8*, 395.
(10) Morita, K.; Sankaran, N. B.; Huang, W. M.; Seino, T.; Sato, Y.; Nishizawa, S.; Teramae, N. *Chem. Commun.* **2006**, 2376.
(11) Morita, K.; Sato, Y.; Seino, T.; Nishizawa, S.; Teramae, N. *Org. Biomol. Chem.* **2008**, *6*, 266.
(12) Santos, P. V. F.; Lopes, I. C.; Diculescu, V. C.; Oliveira-Brett, A. M. *Electroanalysis* **2012**, *24*, 547.
(13) Boon, E. M.; Salas, J. E.; Barton, J. K. *Nat. Biotechnol.* **2002**, *20*, 282.
(14) McWilliams, M. A.; Anka, F. H.; Balkus, K. J.; Slinker, J. D. *Biosens. Bioelectron.* **2014**, *54*, 541.
(15) Zhang, Y.; Zhang, H.; Hu, N. *Biosens. Bioelectron.* **2008**, *23*, 1077.
(16) Chiba, J.; Doi, Y.; Inouye, M. *Res. Chem. Intermed.* **2013**, *39*, 177.
(17) Greco, N. J.; Tor, Y. Z. *Nat. Protoc.* **2007**, *2*, 305.
(18) Cahova-Kucharikova, K.; Fojta, M.; Mozga, T.; Palecek, E. *Anal. Chem.* **2005**, *77*, 2920.
(19) Boon, E. M.; Ceres, D. M.; Drummond, T. G.; Hill, M. G.; Barton, J. K. *Nat. Biotechnol.* **2000**, *18*, 1096.
(20) Gasper, S. M.; Schuster, G. B. *J. Am. Chem. Soc.* **1997**, *119*, 12762.
(21) Giese, B.; Wessely, S. *Chem. Commun.* **2001**, 2108.
(22) Boal, A. K.; Yavin, E.; Lukianova, O. A.; O'Shea, V. L.; David, S. S.; Barton, J. K. *Biochemistry* **2005**, *44*, 8397.
(23) Genereux, J. C.; Barton, J. K. *Chem. Rev.* **2010**, *110*, 1642.
(24) DeRosa, M. C.; Sancar, A.; Barton, J. K. *Proc. Natl. Acad. Sci. U. S. A.* **2005**, *102*, 10788.
(25) Gorodetsky, A. A.; Ebrahim, A.; Barton, J. K. *J. Am. Chem. Soc.* **2008**, *130*, 2924.
(26) Wohlgamuth, C. H.; McWilliams, M. A.; Slinker, J. D. *Anal. Chem.* **2013**, *85*, 1462.
(27) Pheeney, C. G.; Barton, J. K. *J. Am. Chem. Soc.* **2013**, *135*, 14944.
(28) Wohlgamuth, C. H.; McWilliams, M. A.; Slinker, J. D. *Anal. Chem.* **2013**, *85*, 8634.
(29) Slinker, J. D.; Muren, N. B.; Gorodetsky, A. A.; Barton, J. K. *J. Am. Chem. Soc.* **2010**, *132*, 2769.
(30) Slinker, J. D.; Muren, N. B.; Renfrew, S. E.; Barton, J. K. *Nat. Chem.* **2011**, *3*, 228.
(31) Gorodetsky, A. A.; Buzzeo, M. C.; Barton, J. K. *Bioconjugate Chem.* **2008**, *19*, 2285.
(32) Gorodetsky, A. A.; Hammond, W. J.; Hill, M. G.; Slowinski, K.; Barton, J. K. *Langmuir* **2008**, *24*, 14282.
(33) Bard, A. J.; Faulkner, L. R. *Electrochemical methods: fundamentals and applications*; 2nd ed.; Wiley: New York, 2001.
(34) Wohlgamuth, C. H.; McWilliarns, M. A.; Mazaheripour, A.; Burke, A. M.; Lin, K. Y.; Doan, L.; Slinker, J. D.; Gorodetsky, A. A. *J. Phys. Chem. C* **2014**, *118*, 29084.
(35) O'Neill, M. A.; Becker, H. C.; Wan, C. Z.; Barton, J. K.; Zewail, A. H. *Angew. Chem., Int. Ed.* **2003**, *42*, 5896.
(36) Chen, J.; Dupradeau, F. Y.; Case, D. A.; Turner, C. J.; Stubbe, J. *Nucleic Acids Res.* **2008**, *36*, 253.
(37) Chen, J. Y.; Dupradeau, F. Y.; Case, D. A.; Turner, C. J.; Stubbe, J. *Biochemistry* **2007**, *46*, 3096.
(38) Kalnik, M. W.; Chang, C. N.; Grollman, A. P.; Patel, D. J. *Biochemistry* **1988**, *27*, 924.

DOI: 10.1021/jacs.5b06604
J. Am. Chem. Soc. 2015, 137, 11150−11155

(39) Cuniasse, P.; Fazakerley, G. V.; Guschlbauer, W.; Kaplan, B. E.; Sowers, L. C. *J. Mol. Biol.* **1990**, *213*, 303.
(40) Cuniasse, P.; Sowers, L. C.; Eritja, R.; Kaplan, B.; Goodman, M. F.; Cognet, J. A. H.; Lebret, M.; Guschlbauer, W.; Fazakerley, G. V. *Nucleic Acids Res.* **1987**, *15*, 8003.
(41) Hunter, W. N.; Brown, T.; Anand, N. N.; Kennard, O. *Nature* **1986**, *320*, 552.
(42) Brown, T.; Leonard, G. A.; Booth, E. D.; Kneale, G. *J. Mol. Biol.* **1990**, *212*, 437.
(43) Wang, C.; Gao, H.; Gaffney, B. L.; Jones, R. A. *J. Am. Chem. Soc.* **1991**, *113*, 5486.
(44) Dickerson, R. E. *Nucleic Acids Res.* **1989**, *17*, 1797.
(45) O'Dea, J. J.; Osteryoung, J. G. *Anal. Chem.* **1993**, *65*, 3090.
(46) Drummond, T. G.; Hill, M. G.; Barton, J. K. *J. Am. Chem. Soc.* **2004**, *126*, 15010.
(47) Conron, S. M. M.; Thazhathveetil, A. K.; Wasielewski, M. R.; Burin, A. L.; Lewis, F. D. *J. Am. Chem. Soc.* **2010**, *132*, 14388.
(48) Yoo, K. H.; Ha, D. H.; Lee, J. O.; Park, J. W.; Kim, J.; Kim, J. J.; Lee, H. Y.; Kawai, T.; Choi, H. Y. *Phys. Rev. Lett.* **2001**, *87*, 198102.
(49) Marcus, R. A. *Electron Transfer-from Isolated Molecules to Biomolecules*; Jortner, J., Bixon, M., Eds.; Wiley: Hoboken, NJ, 1999; Vol *106*, Part 1, p 1.
(50) Tesar, S. L.; Leveritt, J. M.; Kurnosov, A. A.; Burin, A. L. *Chem. Phys.* **2012**, *393*, 13.

DOI: 10.1021/jacs.5b06604
J. Am. Chem. Soc. 2015, 137, 11150−11155